Nonlinear Dyn
https://doi.org/10.1007/s11071-019-05232-x

ORIGINAL PAPER

Modeling of the nonlinear dynamic degradation characteristics of fiber-reinforced composite thin plates in thermal environment

Hui Li · Tinan Zhang · Zelin Li · Bangchun Wen · Zhongwei Guan

Received: 13 April 2019 / Accepted: 30 August 2019

Abstract In this research, the nonlinear dynamic degradation characteristics of fiber-reinforced composite plates in thermal environment are investigated through a novel dynamic degradation model, which is established by introducing the thermal and time fitting coefficients simultaneously to express dynamic elastic moduli of such composite materials. Based on the classical laminated plate theory, the improved exponential function method, the complex modulus approach and the Ritz method, the dynamic equations are derived to solve the dynamic parameters. Besides, a particle swarm optimization algorithm is employed to iteratively calculate dynamic elastic moduli, and the nonlinear least squares technique in MATLAB software is utilized to draw the three-dimensional fitted surfaces of dynamic elastic moduli, degradation time and temperature data, so that the concerned fitting coefficients in the model developed can be identified. In order to validate the dynamic degradation model, experimental measurements of E120 carbon fiber/ FRD-YG-03 resin composite thin plates are undertaken. The first three natural frequencies, resonant responses and modal damping ratios obtained from the model are compared with experimental results at different degradation time and stabilized thermal environment, which are shown to be in good agreement. Also, the specific influences with and without consideration of the degradation behavior on the dynamic characteristics are investigated and evaluated.

H. Li (✉) · T. Zhang · Z. Li · B. Wen
School of Mechanical Engineering and Automation, Northeastern University, Shenyang 110819, China
e-mail: lh200300206@163.com

T. Zhang
e-mail: ztinan@foxmail.com

Z. Li
e-mail: 1299478310@qq.com

B. Wen
e-mail: bcwen1930@vip.sina.com

H. Li · T. Zhang · Z. Li · B. Wen
Key Laboratory of Vibration and Control of Aero-Propulsion System Ministry of Education, Northeastern University, Shenyang 110819, China

H. Li · Z. Guan
School of Engineering, University of Liverpool, Brownlow Street, Liverpool L69 3GQ, UK
e-mail: Zhongwei.Guan@liverpool.ac.uk

Keywords Dynamic degradation model · Fiber-reinforced composite thin plate · Material nonlinearity · Degradation behavior · Dynamic parameter

1 Introduction

Fiber-reinforced composites are widely used in aeronautical, astronautical, naval vessel and weapon industries due to their light weight and excellent mechanical performance [1,2]. Currently, there are a large number of such composite thin plate structures that are in service in thermal environment, such as composite panels in high-speed aircraft, high-temperature turbine blades in aero engines and composite wings in

Journal: 11071 MS: 5232 TYPESET DISK LE CP Disp.:2019/9/6 Pages: 21 Layout: Medium

the solar unmanned aircraft. Due to the effect of high-temperature environment (which may reach to hundreds or thousands of degrees Celsius), after a period of servicing time, those composite materials and structures will undergo a certain level of dynamic degradation or aging phenomenon [3–5]. This will lead to weakened stiffness and strength, excessive structural vibration, etc.; sometimes even lead to structural function loss, thus causing a possible catastrophic accident for the whole working components and systems.

Usually in the degradation process, the macroscopic dynamic properties of composite materials and structures decline. For example, the natural frequencies and dynamic stiffness decrease gradually [6,7]. Also, some complex changes occur in the vibration stress, dynamic response and damping behavior [8,9]. From the microscopic scale, the dynamic degradation is an irreversible process, which inevitably includes the matrix cracking, delamination damage, interface degradation, inelastic deformation and failure [10–14].

In the past decades, many scholars and researchers mainly focused on the static degradation characteristics of fiber-reinforced composite materials and structures, where the effects of different temperature range and oxidation environment (dry air, fuel gas, water vapor, etc.) on the mechanical degradation properties were studied [11,15–23,25]. For example, McManus [15] proposed an analytical method to calculate stresses and damages in fiber/polymer matrix composites due to the material degradation in thermal environment. Chung et al. [16] established a model by a time–temperature superposition method to predict the degradation effect on the weight of carbon fiber/epoxy composite materials. Zinchenko et al. [17] investigated the effects of thermal degradation of carbon fiber-reinforced plastics and predicted the mass loss based on the physical and mathematical models. Wang et al. [18] conducted an experimental study on the degradation of mechanical properties of carbon and glass fiber-reinforced polyester bars at elevated temperatures. Wolfrum et al. [11] proposed an empiric method that could be used to estimate the degradation of long-term mechanical properties of carbon fiber-reinforced composites in thermal environment based on the experimental data. Dawood and Rizkalla [19] conducted an accelerated environmental exposure tests to evaluate bond strength, yield strength, stiffness degradation of the CFRP systems for strengthening steel structures. Lafarie-Frenot et al. [20] studied the degradation behavior of composite beams in a thermal environment of 150 °C by the numerical model developed. Upadyaya et al. [21] established a mechanism-based multiscale model for degradation prediction of polymer matrix composites at a thermo-oxidative aging condition. Moreover, Bojja et al. [22] predicted the stiffness degradation behavior of GFRP nanocomposites at block amplitude fatigue loads from micro-mechanics. Khalili et al. [23] investigated the effect of thermal cycling from − 30 °C to + 220 °C on the tensile behavior of composite laminate plate. By fitting the electrical impedance measurement results, Ndiaye et al. [24] proposed an acoustical characterization method to quantify the thermal aging behavior of composite plates and honeycomb sandwiches. Guo et al. [25] analyzed the effects of thermal-oxidative aging on the mechanical properties of glass fiber-reinforced polypropylene composites.

To improve the service life of fiber-reinforced materials and structures, the influence of dynamic loads needs to be considered, since the damage possibilities due to vibration loads or other shock loads are often greater than the static loads. Fortunately, some research progresses have been made in this field recently [26–32]. However, most of them only focused on the degradation behavior associated with the increasing environmental temperatures while ignoring the influence of degradation time. For example, Huang and Shen [26] investigated the dynamic behavior of simply supported functionally graded plates in thermal environment. The analytical results revealed that high temperature had an important effect on the reduction of structural natural frequencies. Melo and Radford [27] evaluated the temperature and frequency effects on the viscoelastic properties of fiber-reinforced composites with polymeric matrix (PEEK/IM7 composite). The results showed a decreasing trend in the storage moduli, but an increasing trend in the loss factors as the temperature increased. Based on the temperature-dependent material assumption, Duc et al. [28] established an analytical model to investigate the nonlinear dynamic behavior of the piezoelectric eccentrically stiffened FGM plates in thermal environment. Wu et al. [29] investigated the nonlinear relationships between the dynamic properties and degradation time of the metal and C/SiC plate specimens in high-temperature environment of 1200 °C by finite element simulations and experimental tests. However, only the degradation properties of natural frequencies at different heating time were studied; the changing trends of dynamic responses and damping were not

Journal: 11071 MS: 5232 TYPESET DISK LE CP Disp.:2019/9/6 Pages: 21 Layout: Medium

reported. Jakkamputi and Rajamohan [30] experimentally investigated the natural frequencies and modal damping ratios of CNT-reinforced hybrid polymer composite beams under clamped-free and clamped–clamped boundary conditions when the temperature increased from 30 to 60 °C. Liu et al. [31] measured the time–temperature-dependent elastic moduli of loss factors of CFRP at various temperatures and found that more elastic-like behavior would be induced by the higher frequencies. Based on the experimental and simulation results, Bai et al. [32] studied on the temperature effects on modal parameters of composite honeycomb structure under the suspended boundary condition.

The literature survey presented here indicates that there is limited research work on dynamic degradation modeling techniques of fiber-reinforced composite plates in thermal environment, especially with the lack of systematic analysis and solution of structural resonant responses and damping characteristics. Considering abovementioned issues, this research proposed a novel dynamic degradation model by introducing the thermal and time fitting coefficients simultaneously to express dynamic elastic moduli of such composite materials. Moreover, a particle swarm optimization algorithm with high convergence efficiency and accuracy is employed to iteratively calculate the concerned elastic moduli, which pave a very practical way to facilitate the data fitting operation to identify the key fitting coefficients. Also, a series of experimental tests are conducted to validate the model. The theoretical and experimental findings in this research provide an insight of how the nonlinear dynamic parameters of composite thin plate structures are affected by long-term degradation time over a wide range of stabilized thermal conditions.

2 Modeling and solution

2.1 Description of the dynamic degradation model

Assume that a fiber-reinforced composite thin plate (FCTP), as seen in Fig. 1, which is made of fiber and matrix materials with n layers, is in a uniform thermal environment. First, the coordinate system xyz is set in the mid-plane, and the length, width and thickness are assumed to be a, b and h, respectively. In this theoretical model, the fiber direction within a certain layer is defined as an angle θ from the x-axis of the coordinate,

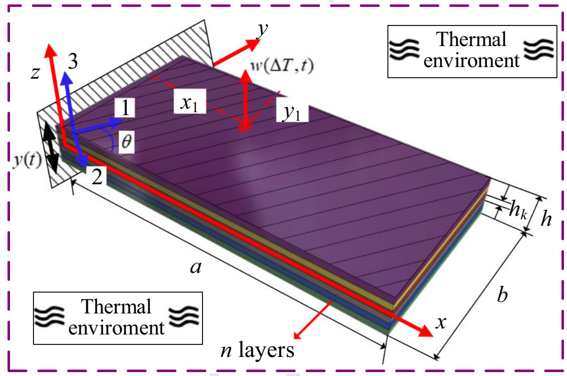

Fig. 1 A theoretical model of fiber-reinforced composite thin plate in thermal environment

and each layer is located between h_{k-1} and h_k along the z-axis with an equal thickness. There is also a local coordinate system, where "1" represents the direction parallel to the fiber, "2" the direction perpendicular to the fiber and "3" the direction perpendicular to the 1–2 plane. In addition, assume that FCTP is under cantilever boundary condition and is subjected to a base excitation load $y(t)$. The concerned vibration displacement $w(\Delta T, t)$ is located at a point (x_1, y_1), which is affected by temperature change ΔT relative to the room temperature (20 °C) and degradation time t (or heating time) simultaneously.

Based on the observed downward trend [33,34] of elastic moduli of fiber-reinforced composite at different temperatures with considering heating time, also utilizing the improved exponential function approach to introduce degradation time t and temperature change ΔT, the dynamic elastic moduli of fiber-reinforced composite materials, $E_1'(\Delta T, t)$, $E_2'(\Delta T, t)$, $G_{12}'(\Delta T, t)$ are assumed to have the following forms

$$E_1'(\Delta T, t) = E_1^R - A_1 \times \Delta T^{B_1} \times e^{-\frac{C_1}{t}} \tag{1}$$

$$E_2'(\Delta T, t) = E_2^R - A_2 \times \Delta T^{B_2} \times e^{-\frac{C_2}{t}} \tag{2}$$

$$G_{12}'(\Delta T, t) = G_{12}^R - A_{12} \times \Delta T^{B_{12}} \times e^{-\frac{C_{12}}{t}} \tag{3}$$

where E_1^R, E_2^R, G_{12}^R represent the elastic moduli in room temperature. To consider the influence caused by thermal environment (or temperature change ΔT), $B_i (i = 1, 2, 12)$ are introduced to represent the thermal fitting coefficients. In addition, to consider the influence due to degradation time t, C_i are introduced to represent the time fitting coefficients. Also, A_i are defined as the adjustment coefficients, which can facilitate the

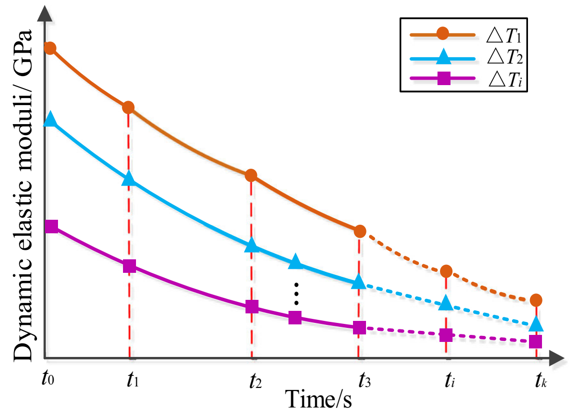

Fig. 2 The schematic diagram of dynamic elastic moduli changed with temperature and degradation time

data fitting operation when the fitting coefficients mentioned above are determined.

The schematic diagram of the change of dynamic elastic moduli with temperature and degradation time is shown in Fig. 2, where ΔT_i $(i = 1, 2, \ldots, k)$ is the temperature difference at each degradation time point.

The complex modulus method is utilized to consider the damping property of fiber-reinforced composites [35,36], according to which their complex dynamic elastic moduli can be further expressed as

$$E_1^*(\Delta T, t) = E_1'(\Delta T, t) \times (1 + \mathrm{i}\eta_1) \tag{4}$$

$$E_2^*(\Delta T, t) = E_2'(\Delta T, t) \times (1 + \mathrm{i}\eta_2) \tag{5}$$

$$G_{12}^*(\Delta T, t) = G_{12}'(\Delta T, t) \times (1 + \mathrm{i}\eta_{12}) \tag{6}$$

where $E_1^*(\Delta T, t)$, $E_2^*(\Delta T, t)$ represent the complex dynamic moduli parallel and perpendicular to the fiber direction in thermal environment, $G_{12}^*(\Delta T, t)$ represents the complex shear modulus, and $\eta_1, \eta_2, \eta_{12}$ are the corresponding loss factors in those fiber directions.

Based on the classical laminated plate theory and the generalized Duhamel–Neumann form of Hooke's Law [37,38], the relationships between stress and strain in the kth layer of FCTP in thermal environment can be expressed as

$$\boldsymbol{\varepsilon}_i^{(k)} = \overline{\boldsymbol{S}}_{ij}^{(k)} \boldsymbol{\sigma}_i^{(k)} + \boldsymbol{\varepsilon}_{\mathrm{T}i}^{(k)} \qquad (i, j = 1, 2, 6) \tag{7}$$

where the stresses are denoted by $\sigma_1 = \sigma_x$, $\sigma_2 = \sigma_y$, $\sigma_6 = \tau_{xy}$. $\boldsymbol{\varepsilon}_i^{(k)}$ are the strains in the kth layer of FCTP, $\boldsymbol{\varepsilon}_{Ti}^{(k)}$ are the thermal strains caused by the thermally induced internal forces, and $\overline{\boldsymbol{S}}_{ij}^{(k)}$ are the partial-axis flexibility coefficient matrix.

The expressions of thermal strains in the kth layer of FCTP are

$$\boldsymbol{\varepsilon}_{\mathrm{T}i}^{(k)} = \begin{bmatrix} \alpha_x \\ \alpha_y \\ \alpha_{xy} \end{bmatrix}^{(k)} \Delta T \quad (i = 1, 2, 12) \tag{8}$$

where α_x, α_y, α_{xy} are the coefficients of thermal expansion along the x, y and shear directions, respectively.

Since θ_k is the fiber angle in the kth layer of FCTP, Φ and Γ are set as $\Phi = \cos\theta_k$ and $\Gamma = \sin\theta_k$ for the convenience of expression. Thus, the relationships between thermal expansion coefficients $\alpha_x, \alpha_y, \alpha_{xy}$ along x, y and shear direction and α_1, .α_2 parallel and perpendicular to the fiber direction can be written as

$$\begin{bmatrix} \alpha_x \\ \alpha_y \\ \alpha_{xy} \end{bmatrix}^{(k)} = \begin{bmatrix} \Phi^2 & \Gamma^2 \\ \Gamma^2 & \Phi^2 \\ 2\Phi\Gamma & -2\Phi\Gamma \end{bmatrix}^{(k)} \begin{bmatrix} \alpha_1 \\ \alpha_2 \end{bmatrix} \tag{9}$$

The stress–strain relationship in any direction of the kth layer of FCTP affected by thermal environment and degradation time can be expressed as follows

$$\begin{bmatrix} \sigma_x \\ \sigma_y \\ \tau_{xy} \end{bmatrix}^{(k)} = \begin{bmatrix} \overline{Q}_{11} & \overline{Q}_{12} & \overline{Q}_{16} \\ \overline{Q}_{12} & \overline{Q}_{22} & \overline{Q}_{26} \\ \overline{Q}_{16} & \overline{Q}_{26} & \overline{Q}_{66} \end{bmatrix}^{(k)} \begin{bmatrix} \varepsilon_x^{(k)} - \varepsilon_{\mathrm{T}x}^{(k)} \\ \varepsilon_y^{(k)} - \varepsilon_{\mathrm{T}y}^{(k)} \\ \gamma_{xy}^{(k)} - \gamma_{\mathrm{T}y}^{(k)} \end{bmatrix} \tag{10}$$

where the strains are denoted by $\varepsilon_1^{(k)} = \varepsilon_x^{(k)}$, $\varepsilon_2^{(k)} = \varepsilon_y^{(k)}$, $\varepsilon_6^{(k)} = \gamma_{xy}^{(k)}$, while the thermal strains are denoted by $\varepsilon_{\mathrm{T1}}^{(k)} = \varepsilon_{\mathrm{T}x}^{(k)}$, $\varepsilon_{\mathrm{T2}}^{(k)} = \varepsilon_{\mathrm{T}y}^{(k)}$, $\varepsilon_{\mathrm{T6}}^{(k)} = \gamma_{\mathrm{T}xy}^{(k)}$. $\overline{\boldsymbol{Q}}_{ij}^{(k)}$ is the partial axis stiffness coefficient matrix in the kth layer of FCTP.

Since $\overline{\boldsymbol{Q}}_{ij}^{(k)}$ incorporates real and imaginary part, it can be expressed in the following form

$$\overline{\boldsymbol{Q}}_{ij}^{(k)} = \overline{\boldsymbol{Q}}_{ij}^{\prime(k)} + \mathrm{i}\overline{\boldsymbol{Q}}_{ij}^{\prime\prime(k)} \tag{11}$$

where $\overline{\boldsymbol{Q}}_{ij}'$ and $\overline{\boldsymbol{Q}}_{ij}''$ are the real and imaginary parts of $\overline{\boldsymbol{Q}}_{ij}^{(k)}$, respectively.

Let $\overline{\boldsymbol{Q}}_{ij}^{(k)} = \boldsymbol{H}^{(k)} \boldsymbol{Q}_{ij} \boldsymbol{H}^{\mathrm{T}(k)}$ (the corresponding expression is shown in "Appendix"). Then, the partial axis stress transformation matrix $\boldsymbol{H}^{(k)}$ in the kth layer of FCTP can be deduced as follows

$$\boldsymbol{H}^{(k)}=\begin{bmatrix}\Phi^2 & \Gamma^2 & 2\Gamma\Phi\\ \Gamma^2 & \Phi^2 & -2\Gamma\Phi\\ -\Gamma\Phi & \Gamma\Phi & \Phi^2-\Gamma^2\end{bmatrix}^{(k)} \tag{12}$$

When the thermal environment and degradation time are both considered, the principal axis stiffness matrix $\boldsymbol{Q}_{ij}$ in all layers of FCTP can be expressed by Poisson's ratio μ_{12}, μ_{21} and the complex dynamic elastic moduli as

$$\boldsymbol{Q}_{ij}=\begin{bmatrix}\frac{E_1^*(\Delta T,t)}{1-\mu_{12}\mu_{21}} & \frac{\mu_{12}E_1^*(\Delta T,t)}{1-\mu_{12}\mu_{21}} & 0\\ \frac{\mu_{21}E_2^*(\Delta T,t)}{1-\mu_{12}\mu_{21}} & \frac{E_2^*(\Delta T,t)}{1-\mu_{12}\mu_{21}} & 0\\ 0 & 0 & G_{12}^*(\Delta T,t)\end{bmatrix} \tag{13}$$

where $\mu_{21}=\mu_{12}\frac{E_2^*(\Delta T,t)}{E_1^*(\Delta T,t)}$.

According to the assumption of the laminated plate theory, the total strain in the kth layer of FCTP is

$$\boldsymbol{\varepsilon}_i^{(k)}=\boldsymbol{\varepsilon}_i^0(x,y,t)+z\boldsymbol{\chi}_i(x,y,t) \tag{14}$$

where $\boldsymbol{\varepsilon}_i^0$ are the mid-plane strains, and $\boldsymbol{\chi}_i$ are the curvatures.

Thus, the relationships between strain and displacement of FCTP can be expressed as

$$\begin{bmatrix}\varepsilon_x^0\\ \varepsilon_y^0\\ \gamma_{xy}^0\end{bmatrix}=\begin{bmatrix}\frac{\partial u^0}{\partial x}\\ \frac{\partial v^0}{\partial y}\\ \frac{\partial u^0}{\partial y}+\frac{\partial v^0}{\partial x}\end{bmatrix},\quad \begin{bmatrix}\chi_x\\ \chi_y\\ \chi_{xy}\end{bmatrix}=-\begin{bmatrix}\frac{\partial^2 w}{\partial x^2}\\ \frac{\partial^2 w}{\partial y^2}\\ \frac{\partial^2 w}{\partial x\partial y}\end{bmatrix} \tag{15}$$

where u^0 and v^0 are the mid-plane displacements in the x and y directions, respectively, and w is the displacement in the z direction.

The overall internal forces and moments can be obtained by integrating the stress of all layers along the z-axis

$$\left(N_x,N_y,N_{xy}\right)=\int_{-h/2}^{h/2}\left(\sigma_x,\sigma_y,\tau_{xy}\right)\mathrm{d}z$$
$$\left(M_x,M_y,M_{xy}\right)=\int_{-h/2}^{h/2}\left(\sigma_x,\sigma_y,\tau_{xy}\right)z\mathrm{d}z \tag{16}$$

Substituting Eq. (14) into Eq. (10) and taking into account of the effects of Eq. (16), the overall internal forces and combined moments of FCTP can be obtained as

$$\begin{bmatrix}\boldsymbol{N}_i\\ \boldsymbol{M}_i\end{bmatrix}=\begin{bmatrix}\boldsymbol{A}_{ij} & \boldsymbol{B}_{ij}\\ \boldsymbol{B}_{ij} & \boldsymbol{D}_{ij}\end{bmatrix}\begin{bmatrix}\boldsymbol{\varepsilon}_i^0\\ \boldsymbol{\chi}_i\end{bmatrix}-\begin{bmatrix}\boldsymbol{N}_{Ti}\\ \boldsymbol{M}_{Ti}\end{bmatrix}(i,j=1,2,6) \tag{17}$$

where $\boldsymbol{N}_{\mathrm{T}i}$, $\boldsymbol{M}_{\mathrm{T}i}$ are the thermally induced internal forces and thermal moments, respectively. $\boldsymbol{A}_{ij}$, $\boldsymbol{B}_{ij}$, $\boldsymbol{D}_{ij}$ are the coefficient matrix. They can be expressed as

$$(\boldsymbol{N}_{\mathrm{T}i},\boldsymbol{M}_{\mathrm{T}i})=\int_{-h/2}^{h/2}\overline{\boldsymbol{Q}}_{ij}\boldsymbol{\alpha}_i\Delta T\,(1,z)\,\mathrm{d}z$$

$$\begin{cases}\boldsymbol{A}_{ij}=\sum_{k=1}^{N}\overline{\boldsymbol{Q}}_{ij}^{(k)}(z_k-z_{k-1})\\ \boldsymbol{B}_{ij}=\frac{1}{2}\sum_{k=1}^{N}\overline{\boldsymbol{Q}}_{ij}^{(k)}(z_k^2-z_{k-1}^2)\\ \boldsymbol{D}_{ij}=\frac{1}{3}\sum_{k=1}^{N}\overline{\boldsymbol{Q}}_{ij}^{(k)}(z_k^3-z_{k-1}^3)\end{cases}$$

2.2 Solutions of the dynamic characteristics with considering degradation behavior

The composite plate is assumed to undergo a base excitation load $y(t)$, which can be regarded as a uniform inertial force loading $q(t)$ with the following expression [39]

$$q(t)=-\rho h\frac{\mathrm{d}^2y(t)}{\mathrm{d}t^2}=\rho hY\omega^2e^{i\omega t} \tag{18}$$

where ρ is the density, Y is the amplitude of base excitation amplitude, and ω is the excitation angular frequency.

By referring to the dynamic equations listed in references [40,41], the equation of vibration displacement of FCTP in thermal environment can be obtained and expressed as

$$\begin{aligned}&4D_{16}\frac{\partial^4 w}{\partial x^3\partial y}+4D_{26}\frac{\partial^4 w}{\partial x\partial y^3}+D_{22}\frac{\partial^4 w}{\partial y^4}-L_1\frac{\partial u^0}{\partial x}\\ &\quad-L_2\frac{\partial u^0}{\partial y}-L_3\frac{\partial v^0}{\partial x}\\ &\quad-L_4\frac{\partial v^0}{\partial y}+L_5\frac{\partial^2 w}{\partial x^2}+\frac{\partial^2 M_{\mathrm{T}x}}{\partial x^2}+2\frac{\partial^2 M_{\mathrm{T}xy}}{\partial x\partial y}\\ &\quad+\frac{\partial^2 M_{\mathrm{T}y}}{\partial y^2}+R\frac{\partial^2 w}{\partial t^2}\\ &=q(t)-N_{\mathrm{T}x}\frac{\partial^2 w}{\partial x^2}-2N_{\mathrm{T}xy}\frac{\partial^2 w}{\partial x\partial y}-N_{\mathrm{T}y}\frac{\partial^2 w}{\partial y^2}\end{aligned} \tag{19}$$

where R is the integral of mass density through the plate thickness, and L_i are the operators with the following expressions

$$L_1=B_{11}\frac{\partial^2}{\partial x^2}+(B_{12}+2B_{66})\frac{\partial^2}{\partial y^2},\ L_2=3B_{16}\frac{\partial^2}{\partial x^2}$$

$$+ B_{26}\frac{\partial^2}{\partial y^2}$$

$$L_3 = B_{16}\frac{\partial^2}{\partial x^2} + 3B_{26}\frac{\partial^2}{\partial y^2},\ L_4 = (B_{12} + 2B_{66})\frac{\partial^2}{\partial x^2} + B_{22}\frac{\partial^2}{\partial y^2}$$

$$L_5 = D_{11}\frac{\partial^2}{\partial x^2} + 2\left(D_{12} + 2D_{66}\right)\frac{\partial^2}{\partial y^2}$$

The concerned composite plate in Fig. 1 is symmetric about the mid-plane, so that the in-plane displacement and out-of-plane displacement are decoupled. Then, according to the small deflection theory of laminate plates, the principle of minimum potential energy and the Ritz method are combined to solve the strain energy V in thermal environment

$$\begin{aligned} V = \frac{1}{2}\int_A \Bigg\{ & D_{11}\left(\frac{\partial^2 w(\Delta T, t)}{\partial x^2}\right)^2 \\ & + 2D_{12}\frac{\partial^2 w(\Delta T, t)}{\partial x^2}\frac{\partial^2 w(\Delta T, t)}{\partial y^2} \\ & + D_{22}\left(\frac{\partial^2 w(\Delta T, t)}{\partial y^2}\right)^2 \\ & + 4D_{16}\frac{\partial^2 w(\Delta T, t)}{\partial x \partial y}\frac{\partial^2 w(\Delta T, t)}{\partial x^2} \\ & + 4D_{26}\frac{\partial^2 w(\Delta T, t)}{\partial x \partial y}\frac{\partial^2 w(\Delta T, t)}{\partial y^2} \\ & + 4D_{66}\left(\frac{\partial^2 w(\Delta T, t)}{\partial x \partial y}\right)^2 \Bigg\} \mathrm{d}A \end{aligned} \tag{20}$$

where A represents the plane area of FCTP.

Considering the influence of thermal environment, the potential energy of the system due to the thermally induced internal forces can be expressed as

$$\begin{aligned} U_{\mathrm{Tem}} = \frac{1}{2}\int_A & N_{\mathrm{T}x}\left(\frac{\partial w(\Delta T, t)}{\partial x}\right)^2 + N_{\mathrm{T}y}\left(\frac{\partial w(\Delta T, t)}{\partial y}\right)^2 \\ & + 2N_{\mathrm{T}xy}\frac{\partial w(\Delta T, t)}{\partial x}\frac{\partial w(\Delta T, t)}{\partial y}\mathrm{d}A \end{aligned} \tag{21}$$

The function of uniform inertial force W_q is

$$W_q = \int\int_A q(t) w(\Delta T, t)\mathrm{d}x\mathrm{d}y \tag{22}$$

The kinetic energy Λ of the system in thermal environment can be expressed as

$$\Lambda = \frac{1}{2}\rho h\int_A \left(\frac{\partial w(\Delta T, t)}{\partial t}\right)^2 \mathrm{d}A \tag{23}$$

Furthermore, the vibration displacement $w(\Delta T, t)$ of a composite thin plate in thermal environment is assumed to be

$$w(\Delta T, t) = W\left(x, y, \Delta T, t\right) e^{\mathrm{i}\omega t} \tag{24}$$

where $W\left(x, y, \Delta T, t\right)$ represents the modal shape function, which can be defined as

$$W\left(x, y, \Delta T, t\right) = \sum_{m=1}^{M}\sum_{n=1}^{N} a_{mn}\left(\Delta T, t\right) X_m\left(x\right) Y_n\left(y\right) \tag{25}$$

where m and n represent the half wave number of the modal shapes along x and y directions, respectively, M and N are the maximum values of m and n. $a_{mn}\left(\Delta T, t\right)$ is the coefficient affected by temperature and degradation time. $X_m\left(x\right)$ and $Y_n\left(y\right)$ are the corresponding modal functions along x and y directions, which can be expressed by the fixed-free beam function and free-free beam function.

Then, according to the Ritz method and neglecting the influence of the harmonic component $e^{\mathrm{i}\omega t}$, the Lagrange energy function $\varPi$ can be defined as

$$\varPi = V + U_{\mathrm{Tem}} - W_q - \Lambda \tag{26}$$

In order to obtain the minimum of the Lagrangian function $\varPi$, Eq. (26) is partially derived with respect to a_{mn} and the following equation can be acquired

$$\frac{\partial V}{\partial a_{mn}} + \frac{\partial U_{\mathrm{Tem}}}{\partial a_{mn}} - \frac{\partial \Lambda}{\partial a_{mn}} = \frac{\partial W_q}{\partial a_{mn}} \tag{27}$$

Substituting Eqs. (20)–(23) into Eq. (27), and letting $\boldsymbol{K}^* = \frac{\partial V}{\partial a_{mn}} + \frac{\partial U_{\mathrm{Tem}}}{\partial a_{mn}}$, $\omega^2\boldsymbol{M} = \frac{\partial \Lambda}{\partial a_{mn}}$, $\boldsymbol{F} = \frac{\partial W_q}{\partial a_{mn}}$, the following equation can be obtained

$$\left(\boldsymbol{K}^* - \omega^2\boldsymbol{M}\right)\boldsymbol{a} = \boldsymbol{F} \tag{28}$$

where $\boldsymbol{M}$ represents the mass matrix of the system, $\boldsymbol{F}$ is excitation force vector, $\boldsymbol{K}^*$ represents the complex stiffness matrix, $\boldsymbol{K}^* = \boldsymbol{K} + \mathrm{i}\boldsymbol{C}$, $\boldsymbol{C}$ represents damping matrix, and $\boldsymbol{a} = (a_{11}, a_{12}, \ldots, a_{mn})^{\mathrm{T}}$ is an eigenvector.

To solve the natural frequency and modal shape, it is only necessary to make the damping matrix $\boldsymbol{C}$ and excitation force vector $\boldsymbol{F}$ equal to zero

Journal: 11071 MS: 5232 TYPESET DISK LE CP Disp.:2019/9/6 Pages: 21 Layout: Medium

$$\left(\boldsymbol{K}-\omega^2\boldsymbol{M}\right)\boldsymbol{q}=0 \tag{29}$$

By solving Eq. (29), the natural frequencies of FCTP affected by temperature and degradation time can be obtained. Then, by substituting the eigenvector $\boldsymbol{q}=(q_{11},q_{12},\ldots q_{mn})^{\mathrm{T}}$ into Eq. (25), the concerned modal shapes can also be obtained.

Consequently, the coefficient matrix $\boldsymbol{a}_{mn}$ can be expressed as

$$\boldsymbol{a}_{mn}=\left[\boldsymbol{K}^{*}-\omega^2\boldsymbol{M}\right]^{-1}\boldsymbol{F} \tag{30}$$

Substitute the vector $\boldsymbol{a}_{mn}$ into Eq. (25) and then into Eq. (24), and set $e^{\mathrm{i}\omega t}=1$, the concerned vibration displacement $w(\Delta T,t)$ can be obtained.

Considering that usually the absolute vibration response $\lambda(\Delta T,t)$ of a composite structure is obtained in experimental tests, it should include the structural vibration response $w(\Delta T,t)$ and the base excitation displacement $y(t)$. Therefore, $\lambda(\Delta T,t)$ can be further expressed as

$$\lambda(\Delta T,t)=y(t)+w(\Delta T,t) \tag{31}$$

The total strain energy $\overline{V}_i$ in the ith mode of FCTP affected by temperature and degradation time can be expressed as

$$\overline{V}_i=\overline{V}(i,x)+\overline{V}(i,y)+\overline{V}(i,xy)+\overline{V}(i,\Delta T) \tag{32}$$

where $\overline{V}(i,x)$, $\overline{V}(i,y)$, $\overline{V}(i,xy)$ represent the corresponding ith strain energy along the x, y, and xy directions respectively and $\overline{V}(i,\Delta T)$ is the ith potential energy caused by thermally induced internal forces.

$$\begin{aligned}
\overline{V}(i,x)&=\frac{1}{2}\sum_{k=1}^{N}\int_{h_{k-1}}^{h_k}\int_A\overline{\boldsymbol{Q}}'_{ij}\left(\varepsilon_x-\varepsilon_{\mathrm{T}x}\right)\varepsilon_x\mathrm{d}A\mathrm{d}z\\
\overline{V}(i,y)&=\frac{1}{2}\sum_{k=1}^{N}\int_{h_{k-1}}^{h_k}\int_A\overline{\boldsymbol{Q}}'_{ij}\left(\varepsilon_y-\varepsilon_{\mathrm{T}y}\right)\varepsilon_y\mathrm{d}A\mathrm{d}z\\
\overline{V}(i,xy)&=\frac{1}{2}\sum_{k=1}^{N}\int_{h_{k-1}}^{h_k}\int_A\overline{\boldsymbol{Q}}'_{ij}\left(\gamma_{xy}-\gamma_{\mathrm{T}xy}\right)\gamma_{xy}\mathrm{d}A\mathrm{d}z\\
\overline{V}(i,\Delta T)&=\frac{1}{2}\int_A N'_{\mathrm{T}x}\left(\frac{\partial w(\Delta T,t)}{\partial x}\right)^2\\
&\quad+N'_{\mathrm{T}y}\left(\frac{\partial w(\Delta T,t)}{\partial y}\right)^2\\
&\quad+2N'_{\mathrm{T}xy}\frac{\partial w(\Delta T,t)}{\partial x}\frac{\partial w(\Delta T,t)}{\partial y}\mathrm{d}A
\end{aligned}$$

where $N'_{\mathrm{T}x}$, $N'_{\mathrm{T}y}$, $N'_{\mathrm{T}xy}$ can be obtained by solving the real part of complex stiffness matrix coefficients $\overline{\boldsymbol{Q}}'_{ij}$ in Eqs (11) and (17).

The total dissipated energy $\Delta\overline{V}_i$ in the ith mode of FCTP affected by temperature and degradation time can be expressed as

$$\Delta\overline{V}_i=\Delta\overline{V}(i,x)+\Delta\overline{V}(i,y)+\Delta\overline{V}(i,xy)+\Delta\overline{V}(i,\Delta T) \tag{33}$$

where $\Delta\overline{V}(i,x)$, $\Delta\overline{V}(i,y)$ and $\Delta\overline{V}(i,xy)$ represent the corresponding ith dissipated energy along the x, y and xy directions, respectively, and $\Delta\overline{V}(i,\Delta T)$ is the ith dissipated energy caused by thermally induced internal forces.

$$\begin{aligned}
\Delta\overline{V}(i,x)&=\pi\sum_{k=1}^{N}\int_{h_{k-1}}^{h_k}\int_A\overline{\boldsymbol{Q}}''_{ij}\left(\varepsilon_x-\varepsilon_{\mathrm{T}x}\right)\varepsilon_x\mathrm{d}A\mathrm{d}z\\
\Delta\overline{V}(i,y)&=\pi\sum_{k=1}^{N}\int_{h_{k-1}}^{h_k}\int_A\overline{\boldsymbol{Q}}''_{ij}\left(\varepsilon_y-\varepsilon_{\mathrm{T}y}\right)\varepsilon_y\mathrm{d}A\mathrm{d}z\\
\Delta\overline{V}(i,xy)&=\pi\sum_{k=1}^{N}\int_{h_{k-1}}^{h_k}\int_A\overline{\boldsymbol{Q}}''_{ij}\left(\gamma_{xy}-\gamma_{\mathrm{T}xy}\right)\gamma_{xy}\mathrm{d}A\mathrm{d}z\\
\Delta\overline{V}(i,\Delta T)&=\pi\int_A N''_{\mathrm{T}x}\left(\frac{\partial w(\Delta T,t)}{\partial x}\right)^2\\
&\quad+N''_{\mathrm{T}y}\left(\frac{\partial w(\Delta T,t)}{\partial y}\right)^2\\
&\quad+2N''_{\mathrm{T}xy}\frac{\partial w(\Delta T,t)}{\partial x}\frac{\partial w(\Delta T,t)}{\partial y}\mathrm{d}A
\end{aligned}$$

where $N''_{\mathrm{T}x}$, $N''_{\mathrm{T}y}$, $N''_{\mathrm{T}xy}$ can be obtained by solving the imaginary part of complex stiffness matrix coefficients $\overline{\boldsymbol{Q}}'_{ij}$ in Eqs (11) and (17).

Finally, the ith modal damping ratio of FCTP with considering degradation behavior in thermal environment can be expressed as

$$\xi_i=\frac{\Delta\overline{V}_i}{4\pi\overline{V}_i} \tag{34}$$

Journal: 11071 MS: 5232 TYPESET DISK LE CP Disp.:2019/9/6 Pages: 21 Layout: Medium

3 Determination of the fitting coefficients in the theoretical model

Because thermal environment has a great influence on composite material parameters, here the identification principle of dynamic elastic moduli is described by combining theory with practice, which is a prerequisite for determining the concerned fitting coefficients at different temperatures and degradation time points.

3.1 Iterative calculations of dynamic elastic moduli

In this section, due to the high convergence efficiency, small computational complexity [42], a particle swarm optimization algorithm (PSOA) is employed to iteratively calculate the dynamic elastic moduli of fiber-reinforced composites, so as to obtain the theoretical natural frequency data to approach to the experimental natural frequency data. In the PSOA, firstly, a D-dimensional target search space (or D optimal value) needs to be chosen, and a group can be formed through I particles whose positions are randomly assigned (to get the random solution). Then, each particle $\boldsymbol{X}_i$, which contains the dynamic elastic moduli of composite plate, can be expressed as

$$\boldsymbol{X}_i = [\boldsymbol{E}'_1, \boldsymbol{E}'_2, \boldsymbol{G}'_{12}] \qquad (i = 1, 2, \ldots I) \tag{35}$$

where

$$\boldsymbol{E}'_1 = \left[E_1^1,\ E_1^2,\ E_1^3,\ \ldots,\ E_1^I\right]$$
$$\boldsymbol{E}'_2 = \left[E_2^1, E_2^2, E_2^3,\ \ldots,\ E_2^I\right]$$
$$\boldsymbol{G}'_{12} = \left[G_{12}^1, G_{12}^2, G_{12}^3,\ \ldots, G_{12}^I\right]$$

In each iterative calculation, the particle updates itself by tracking the two "extreme values" at velocity $\boldsymbol{V}_i$. Here, the first extreme value is the best solution the particle itself can find, called the individual extremum point (representing its position with p_b). In the global version of the PSOA [43], the other extreme point in the population is the best solution currently found for the entire population, called the global extreme point (with G_b for its position).

Then, some new points are chosen by adding $\boldsymbol{V}_i$ coordinates to $\boldsymbol{X}_i$, and the algorithm operates by adjusting $\boldsymbol{V}_i$, which can be seen as an effective step size. At the meantime, the particle $\boldsymbol{X}_i$ updates its speed and position according to the following rules:

$$\begin{aligned}\boldsymbol{V}_i^{k+1} &= \varpi \times \boldsymbol{V}_i^k + c_1^p \times rand_1^k(p_b[i] - \boldsymbol{X}_i)\\ &\quad + c_2^p \times rand_2^k(G_b[i] - \boldsymbol{X}_i)\end{aligned} \tag{36}$$

$$\boldsymbol{X}_i^{k+1} = \boldsymbol{X}_i^k + \boldsymbol{V}_i^{k+1} \tag{37}$$

where c_1^p and c_2^p is the learning factors, $rand()$ is a matrix of random numbers over [0, 1], and ϖ is the inertia weight.

During the calculation process in the PSOA, each column element of $\boldsymbol{X}_i$ is randomly obtained within the range of $\boldsymbol{E}'_1, \boldsymbol{E}'_2, \boldsymbol{G}'_{12}$. Firstly, to consider the effects of thermal environment with degradation time, elastic moduli in different fiber directions are assumed to be variable. Then, set the elastic moduli at room temperature as the base values (such as $E_1^{\mathrm{R}}, E_2^{\mathrm{R}}, G_{12}^{\mathrm{R}}$) and take into account the possible error R_{err} generated by the temperature change (usually $R_{\mathrm{err}} = 50\%$ is large enough). In this way, the range of $\boldsymbol{E}'_1, \boldsymbol{E}'_2, \boldsymbol{G}'_{12}$ at certain time point and temperature condition can be determined as follows

$$\begin{aligned}E_1^{\mathrm{R}}\,(1 - R_{\mathrm{err}}) &\le E'_1(\Delta T, t) \le E_1^{\mathrm{R}}\,(1 + R_{\mathrm{err}})\\ E_2^{\mathrm{R}}\,(1 - R_{\mathrm{err}}) &\le E'_2(\Delta T, t) \le E_2^{\mathrm{R}}\,(1 + R_{\mathrm{err}})\\ G_{12}^{\mathrm{R}}\,(1 - R_{\mathrm{err}}) &\le G'_{12}(\Delta T, t) \le G_{12}^{\mathrm{R}}\,(1 + R_{\mathrm{err}})\end{aligned} \tag{38}$$

Consequently, the position of the particle $\boldsymbol{X}_i$ is used to represent the optimal solution of the elastic modulus parameters. The performance of each particle $\boldsymbol{X}_i$ depends on the fitness error value e_{fre} (usually should be set as $e_{\mathrm{fre}} \le 5\%$), which can be determined by an error function between the theoretical and measured results described as follows.

$$e_{\mathrm{fre}} = \sum_i^{R_m} \left(\frac{f_i - \hat{f}_i}{\hat{f}_i}\right) \Big/ R_m \tag{39}$$

where R_m represents the number of modes in the concerned frequency range, f_i represents the ith natural frequency obtained by the calculations, $\hat{f}_i$ is the ith natural frequency obtained by the experimental tests.

If the minimum error requirement in Eq. (32) can be met, the iterative calculation process is terminated and the optimal solutions are obtained. By repeating the above steps, the optimal elastic moduli at different degradation time points and thermal environment can be obtained.

Journal: 11071 MS: 5232 ☐ TYPESET ☐ DISK ☐ LE ☐ CP Disp.:2019/9/6 Pages: 21 Layout: Medium

3.2 Identification of the fitting coefficients of dynamic elastic moduli

Since the concerned fitting coefficients of dynamic elastic moduli, A_i, B_i and C_i are dependent to the temperature and time, the nonlinear least squares technique is used in the Curve Fitting Tool (CFtool) in MATLAB software to fit the three dimensional curves.

Firstly, the temperature, degradation time and elastic modulus data are inputted and written in matrix forms. Then, when these data are read by the CFtool interface, "X data" is set to represent temperature, "Y data" to degradation time, and "Z data" to dynamic elastic moduli in the drop-down menu. (But, Z data can only be one kind of dynamic elastic moduli each time.) Usually, CFtool has various function fitting tools, including Custom Equation, Interpolant, Polynomial, etc. Here, considering the downward trend in changing of dynamic elastic modulus, "Custom Equation" is employed to draw the 3D fitted surfaces of dynamic elastic moduli at different degradation time points and thermal environments, which could better show their nonlinear relationships. Also, this fitting tool can help to automatically calculate the initial values of A_i, B_i and C_i when the 3D fitted surfaces are obtained. In addition, it should be noted that in order to determine the optimal fitting coefficients, "R-square" value in the CFtool interface should be calculated repeatedly, which is within the range of [0, 1]. The closer to 1 it is, the more accurate values of A_i, B_i and C_i are obtained. The expression of "R-square" can be written as follows [44].

$$R_{\text{square}} = 1 - \frac{\sum_{i=1}^{N_{\text{data}}} (\hat{y}_i - \overline{y}_i)^2}{\sum_{i=1}^{N_{\text{data}}} (y_i - \overline{y}_i)^2} \tag{40}$$

where y_i is original data, $\overline{y}_i$ is the average of y_i, $\hat{y}_i$ is the fitting data, and N_{data} represents the total number of y_i.

4 A case study

In this section, five E120 carbon fiber/ FRD-YG-03 resin composite thin plates were taken as the research subjects. Three plate specimens were used to measure the varied natural frequencies at different temperatures and degradation time points, so as to obtain the fitting coefficients of dynamic elastic moduli in the degradation model. The other two plates with different sizes but the same material parameters were used to verify the theoretical model.

4.1 Test specimens and test system

In order to ensure a good test reliability, three plate specimens with the same size, namely composite A, B and C, were taken as test objects. They were cut from a large composite plate laminated and produced by Weisheng Xincai Composite Materials Co. Ltd. Each plate has total 15 layers with lamination configurations of $[(0°/90°)_3/0°/90°/0°/(90°/0°)_3]$, which is symmetrically laid, with a longitudinal elastic modulus of 120 GPa, transverse elastic modulus of 11.32 GPa, shear modulus of 7.13 GPa, Poisson's ratio of 0.32, a density of 1693.2 kg/m^3 and loss factors $\eta_1 = 0.0063$, $\eta_2 = 0.0074$, $\eta_{12} = 0.0089$ in the room temperature. (Those material parameters are provided by the company.) The length is 260 mm, width is 130 mm and thickness is 2.13 mm. The thermal expansion coefficients parallel and perpendicular to the fiber direction are -0.15×10^{-6}/°C and 1.1×10^{-6}/°C, respectively.

A dynamic degradation test system in thermal environment was set up, as shown in Fig. 3, to measure the varied natural frequencies, vibration responses and damping parameters in different temperatures and heating time points. In the experiment, the clamping fixture with four M8 bolts was used to clamp the plate specimen firmly (with a clamping width of 30 mm along the x-axis of the specimen) to simulate the cantilever boundary condition (seen in Fig. 3). The laser measuring point was 70 mm to the constraint end of the plate specimen, while the horizontal distance between this point and the right free edge was 30 mm.

The instruments and sensors used in the dynamic degradation measurements are listed in Table 1. The heating box with two thermocouple sensors was used to provide the required temperature, which can be adjusted by temperature control device. (Here, one thermocouple was used to measure the temperature within the heating box, and the other one was connected to the temperature control device for feedback purpose.)

On top of the box was an insulated glass plate through which the laser beam generated by the Polytec PDV-100 laser Doppler vibrometer can measure the vibration response on the plate specimens. The

Journal: 11071 MS: 5232 TYPESET DISK LE CP Disp.:2019/9/6 Pages: 21 Layout: Medium

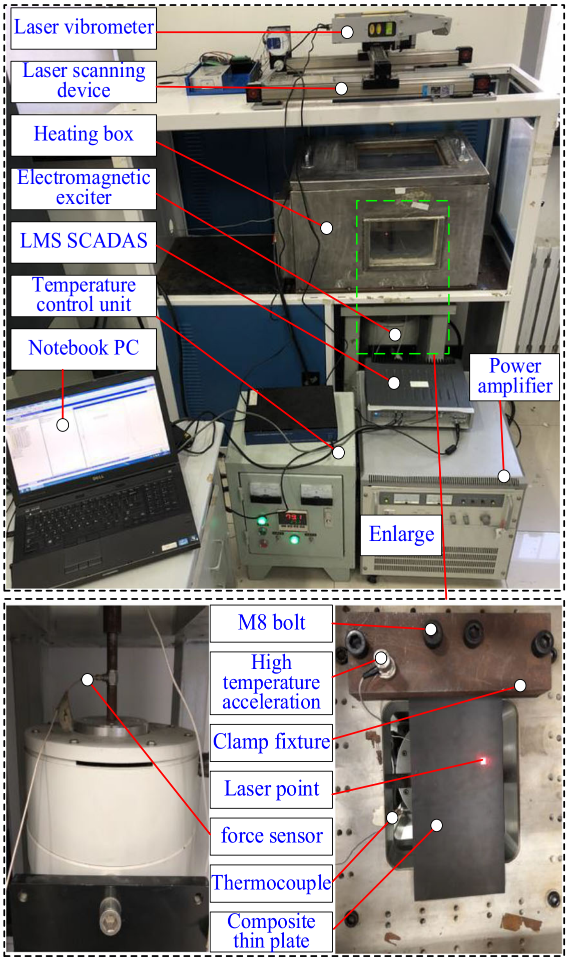

Fig. 3 A dynamic degradation test system of composite thin plates in thermal environment

motion of the laser point was powered by the two-dimensional laser scanning device controlled by LabVIEW software, which greatly improved the test efficiency, especially on the modal shape measurements in thermal condition [45]. The electromagnetic exciter and power amplifier (which were placed outside of the heating box) were employed to generate basic excitation load, which can be measured with a high-temperature accelerometer at room temperature (20 °C) or in high-temperature environment. Besides, a force sensor located at the middle of the rod of the electromagnetic exciter was used to determine the effectiveness of exciting energy and also to avoid excessive excitation energy (so that negative effects caused by the geometric nonlinear vibration of the specimen can be eliminated). All of the acceleration, force and

Table 1 The instruments and sensors used in the dynamic degradation measurements

Order	Hardware type	Model
1	Laser Doppler vibrometer	Polytec PDV-100
2	Two-dimensional laser scanning device	Self-designed
3	Electromagnetic exciter	Lianneng JZK-100
4	Power amplifier	Lianneng YE5878
5	Force sensor	PCB 200B01
6	High temperature accelerometer	Lianneng CL-YD-301
7	Heating box	Changbai T-500
8	Thermocouple sensor	Yongyang PT100
9	Temperature control device	Changbai C-500
10	Modal hammer	PCB086101
11	Data acquisition instrument	LMS SCADAS 16-channel front-end
12	Mobile workstation	DELL precision M6600

temperature signals were recorded and stored by LMS SCADAS 16-channel data acquisition front-end and the notebook computer. (The output channel of LMS SCADAS was also used to generate vibration excitation signal to electromagnetic exciter.)

4.2 Identification of fitting coefficients

Firstly, the composite plates *A*, *B* and *C* were installed firmly in the clamping fixture. Based on the test system established, sine sweeping excitation tests were performed at room temperature with a frequency range of 0–550 Hz, a frequency resolution of 0.25 Hz, an excitation amplitude of 1 g and a sweeping speed of 1 Hz/s. After measuring the raw response signal, the small-segment FFT processing technique [46] was employed to obtain frequency spectrum of the response signal. The natural frequencies of those specimens were determined by identifying the response peaks in these spectrums.

Next, the heating box was utilized to provide the plate specimens mentioned above with different thermal environments (i.e., plate *A* at 100 °C, plate *B* at 150 °C and plate *C* at 200 °C, respectively). Natural frequencies at different degradation time points and temperatures were obtained by the sweeping excitation

Journal: 11071 MS: 5232 TYPESET DISK LE CP Disp.:2019/9/6 Pages: 21 Layout: Medium

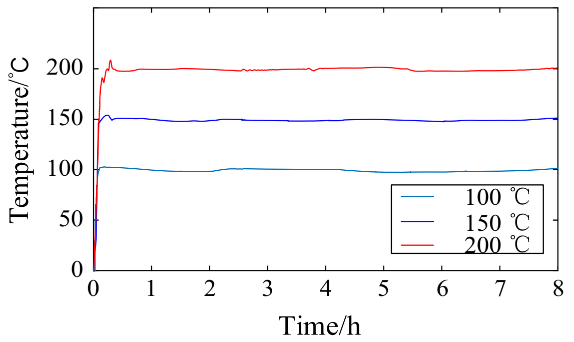

Fig. 4 The measured heating curve of composite plate C varied with the time in the heating box

technique similar as that of the room temperature test. It should be noted that each heating process was kept for more than 6 hours. Dynamic degradation experiments were performed at an interval of two hours to measure the natural frequencies. Besides, the experimental data were acquired only when the temperature was in a stabilized phase rather than a rising phase. Take the degradation test of composite plate C as an example. The temperature versus time curve is shown in Fig. 4. Temperature ascended at the beginning and stabilized after a certain period of time when the data recorded were valid. In this way the poor control effect in short-term heating and unwanted influence of temperature fluctuation could be exclude. It should be noted that we try to focus on the long-term degradation test of FCTP in different stabilized thermal environments. Here, the measured natural frequencies of three composite plate specimens with varied degradation time at 100 °C, 150 °C and 200 °C are listed in Tables 2, 3 and 4.

Then, according to the PSOA described in Sect. 3.1, set the following parameters in the self-written MATLAB program: (1) particle population number: 20; (2) learning factor $c_1 = c_2 = 2$; (3) the maximum number of iterations: 1000; (4) inertia weight $\varpi = 0.9$. In the iterative calculation process, if the error calculation formula [Eq. (39)] was satisfied, the execution of the program would be terminated, and the optimal particle $\boldsymbol{X}_i$, which contained the dynamic elastic moduli would be outputted. In order to compare the theoretical predictions with the test results, the iteratively calculated natural frequencies of three composite plate specimens at different degradation time points and thermal environments (100 °C, 150 °C and 200 °C) are listed in Tables 2, 3 and 4. It can be seen that the calculation errors of natural frequencies are no more than 9.2%. Therefore, the corresponding dynamic elastic moduli of fiber-reinforced composite can be extracted in CFtool in MATLAB software. Table 5 lists the identified results of E_1', E_2', G_{12}' at different degradation time points and temperatures. (The identified results at room temperature are also provided, which are very close to the ones the manufacturer provided in Sect. 4.1.)

Then, the result data in Table 5 are used to draw the 3D fitted surfaces of dynamic elastic moduli at different degradation time points and thermal environments, as shown in Fig. 5. Through analyzing the degradation phenomenon from Fig. 5, it can be observed that the dramatic degradation change of elastic moduli of the chosen composite plate specimens in thermal environment occurs in the first 2 hours. The reason may be that there is a big change of temperature value in this stage (the heating process), so the macroscopic softening effect on composite plate is obvious, which subsequently leads to the dramatical reduction of elastic moduli. Then, as the plate structure is already within a constant thermal environment (the temperature value is keeping at a fixed level), in the following 4 h, 6 h and 8 h, the degradation performance of dynamic elastic moduli is developed relatively slowly. It should be noted due to the time-consuming and high-cost of experimental tests, the further degradation test (lasting one day or several days) were not conducted. However, based on the analysis conclusion in literatures [35,47], the development of degradation behavior would continue for a long time.

Finally, by substituting the identified fitting coefficients (as listed in Table 6) into Eqs. (1)–(3), the expressions of dynamic elastic moduli in thermal environment with degradation time can be obtained

$$E_1'(\Delta T, t) = 120.612 - 1.806 \times \Delta T^{0.6651} \times e^{-\frac{0.3338}{t}}$$

$$E_2'(\Delta T, t) = 10.882 - 0.001864 \times \Delta T^{1.432} \times e^{-\frac{0.5421}{t}}$$

$$G_{12}'(\Delta T, t) = 6.785 - 0.00147 \times \Delta T^{1.476} \times e^{-\frac{0.2996}{t}}$$

4.3 Comparison and verification of the inherent characteristics

In this section, in order to verify the correctness of the theoretical model, the composites plate D and plate E were used for calculation and test. Their length, width and thickness were 330 mm × 130 mm × 2.36 mm.

Journal: 11071 MS: 5232 TYPESET DISK LE CP Disp.:2019/9/6 Pages: 21 Layout: Medium

Table 2 Natural frequencies of composite plate A obtained by tests and iterative calculations with varied degradation time at 100 °C

Type	Degradation time/h	Mode 1	Mode 2	Mode 3	Mode 4
Experiment $\hat{f}_i$/Hz	0 (room temperature)	39.5	97.7	238.9	328.3
	2	37.3	94.8	227.5	310.8
	4	37.0	93.5	227.4	308.1
	6	36.8	92.8	224.2	305.5
	8	36.8	92.3	224.0	302.5
Calculation f_i/Hz	0 (room temperature)	41.3	99.4	253.7	339.4
	2	37.4	98.3	241.4	322.6
	4	37.1	97.2	238.5	318.1
	6	36.8	96.9	235.7	314.0
	8	36.5	96.6	232.3	310.4
Error $\left\|\hat{f}_i - f_i\right\| / \hat{f}_i$/%	0 (room temperature)	4.6	1.7	6.2	3.4
	2	0.3	3.7	6.1	3.8
	4	0.3	4.0	4.9	3.2
	6	0	4.4	5.1	2.8
	8	0.8	4.7	3.7	2.6

Table 3 Natural frequencies of composite plate B obtained by tests and iterative calculations with varied degradation time at 150 °C

Type	Degradation time/h	Mode 1	Mode 2	Mode 3	Mode 4
Experiment $\hat{f}_i$/Hz	0 (room temperature)	37.2	96.8	228.0	322.1
	2	35.0	93.3	211.5	307.0
	4	34.5	92.8	210.0	305.5
	6	33.3	91.7	209.8	302.0
	8	31.5	91.3	208.3	300.2
Calculation f_i/Hz	0 (room temperature)	40.5	98.1	233.7	334.4
	2	35.3	97.8	221.6	316.9
	4	35.0	96.8	214.0	309.3
	6	34.6	96.5	211.6	305.8
	8	34.4	96.3	209.8	302.5
Error $\left\|\hat{f}_i - f_i\right\| / \hat{f}_i$/%	0 (room temperature)	8.9	1.3	2.5	3.8
	2	0.9	4.8	4.8	3.2
	4	1.4	4.3	1.9	1.2
	6	3.9	5.2	0.9	1.3
	8	9.2	5.5	0.7	0.8

After the plate specimen was firmly clamped, the effective dimensions of length, width and thickness were 300 mm × 130 mm × 2.36 mm. The laser measuring point was placed at the same position as that of composite plates A, B and C.

In the test, the heating temperature was chosen as 120 °C for plate D and 180 °C for plate E. Four degradation time points of 0 h, 2 h, 4 h and 6 h were selected. The similar sine excitation method and signal data processing and identification techniques described in Sect. 4.2 were utilized to measure the first three natural frequencies of the two plate specimens, as listed in Tables 7 and 8. In addition, the laser linear scanning method [47] was used to measure modal shapes. Taking the measurement of composite plate D as an example,

Journal: 11071 MS: 5232 TYPESET DISK LE CP Disp.:2019/9/6 Pages: 21 Layout: Medium

Table 4 Natural frequencies of composite plate C obtained by tests and iterative calculations with varied degradation time at 200 °C

Type	Degradation time/h	Mode 1	Mode 2	Mode 3	Mode 4
Experiment $\hat{f}_i$/Hz	0 (room temperature)	36.8	94.5	223.9	312.5
	2	32.6	91.6	211.5	300.3
	4	30.8	89.3	208.5	299.7
	6	29.8	88.4	208.0	297.3
	8	29.3	87.5	207.5	296.0
Calculation f_i/Hz	0 (room temperature)	39.8	96.1	228.5	329.4
	2	33.7	92.9	216.5	310.1
	4	32.0	91.1	212.3	307.7
	6	31.6	90.4	210.9	305.3
	8	31.3	89.8	209.2	301.6
Error $\left\lvert \hat{f}_i - f_i \right\rvert / \hat{f}_i$/%	0 (room temperature)	8.2	1.7	2.1	5.4
	2	3.4	1.4	2.4	3.3
	4	3.9	2.0	1.8	2.7
	6	6.0	2.3	1.4	2.7
	8	6.8	2.6	0.8	1.9

Table 5 The identified dynamic elastic moduli of E120 carbon fiber/FRD-YG-03 resin composite at different degradation time points and thermal environments

Temperature/°C	Type	Degradation time/h			
		2	4	6	8
Room temperature	E_1'/Gpa	120.612	120.612	120.612	120.612
	E_2'/Gpa	10.882	10.882	10.882	10.882
	G_{12}'/Gpa	6.785	6.785	6.785	6.785
100	E_1'/Gpa	92.875	90.514	87.979	85.106
	E_2'/Gpa	9.783	9.632	9.587	9.490
	G_{12}'/Gpa	5.571	5.395	5.232	5.140
150	E_1'/Gpa	72.110	70.351	67.905	66.529
	E_2'/Gpa	8.987	8.794	8.612	8.523
	G_{12}'/Gpa	5.020	4.904	4.830	4.762
200	E_1'/Gpa	71.021	69.212	66.702	64.830
	E_2'/Gpa	7.912	7.599	7.406	7.246
	G_{12}'/Gpa	3.415	3.382	3.207	3.110

the first three modal shapes with varied degradation time at 120 °C were obtained, as shown in Table 9.

Then, set the same heating temperatures and degradation time points to calculate the natural frequencies based on the theoretical model established. The corresponding calculation results and errors of plate D and plate E are listed in Tables 7 and 8. For the convenience to compare, the calculated natural frequencies and the resulting errors without considering the degradation effect are also listed in the same tables. Besides, Table 9 shows the calculated modal shape results of composite plate D. Based on the work carried out by Jeyaraj et al. [8] and Li et al. [48], the modal shapes of composite plates seem to be immune to temperatures; hence, there is no need to discuss the degradation effect on modal shapes.

It can be seen from Tables 7, 8 and 9 that there is a good agreement between the calculated and measured natural frequencies at different degradation time points in those thermal environments, which is evi-

Journal: 11071 MS: 5232 TYPESET DISK LE CP Disp.:2019/9/6 Pages: 21 Layout: Medium

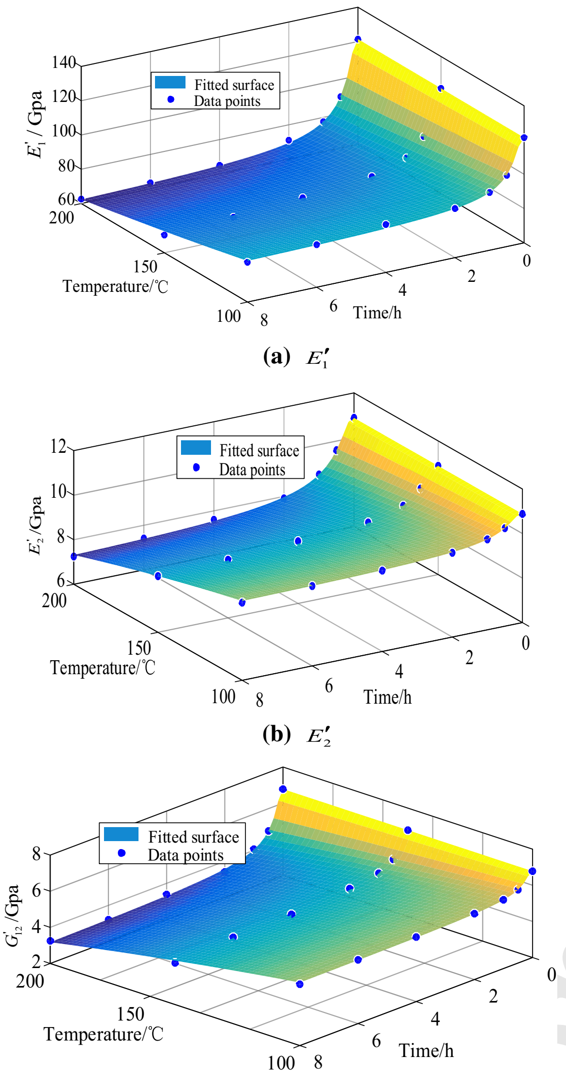

(a) E_1'

(b) E_2'

(c) G_{12}'

Fig. 5 The 3D fitted surfaces of dynamic elastic moduli at different degradation time points and thermal environments

denced by the calculation errors of the first 3 natural frequencies of FCTP at 120 °C and 180 °C being less than 9.6% with considering the degradation effect. The morphological characteristics of the calculated and measured modal shapes also agree well. However, the natural frequencies calculated without considering the degradation effect have a larger error. What's more, the longer the degradation time is, the greater the error. For example, when the temperature is raised to 180 °C, the maximum calculation error of the first 3 natural frequencies at the degradation time point of 6 h reaches

Table 6 The identified fitting coefficients of fiber-reinforced composites

Type	Fitting coefficient	Value
E_1'	A_1	1.806
	B_1	0.6651
	C_1	0.3338
E_2'	A_2	0.001864
	B_2	1.432
	C_2	0.5421
G_{12}'	A_{12}	0.00147
	B_{12}	1.476
	C_{12}	0.2996

to 21.1%, while the maximum error at the degradation time point of 2 h is 16.5%. Therefore, it is necessary to introduce the material nonlinearity in the modeling process, and the degradation model proposed improves the calculation accuracy of natural frequencies of FCTP.

Furthermore, by comparing the measured natural frequencies of composite thin plate structures at different thermal environments, it can be found out that the higher the temperature is, the more severe degradation phenomenon of FCTP is induced, especially when the environmental temperature is raised from room temperature to a higher temperature through the first heating process for 2 hours. By taking the first natural frequency as an example, the reduced magnitude at degradation time point of 2 h at 120 °C is 17.3%, while the corresponding reduced magnitude reaches to 28.1% when the temperature becomes to 180 °C. The reason for this phenomenon may be due to a big reduction in structural stiffness of FCTP caused by the sharp variation of thermal environment. However, with the degradation time lasting, as the thermal environment gets increasingly stabilized, the composite plate structure shows a slowed downward trend in changing of natural frequency, i.e., the stiffness softening effect due to degradation effect becomes smaller and smaller.

4.4 Comparison and verification of the dynamic response

Here, the first three resonant responses at different degradation time points at 120 °C and 180 °C were measured when the base excitation amplitude of 1g

Table 7 The measured and calculated natural frequencies of composite plate D with varied degradation time at 120 °C as well as the calculation errors with and without considering degradation behavior

Time/h	Type	Mode 1	Mode 2	Mode 3
0 (Room temperature)	Experiment $\hat{f}_i$/Hz	24.8	73.6	155.0
	Calculation f_i/Hz	25.9	75.2	162.4
	Error $\left\|\hat{f}_i - f_i\right\| / \hat{f}_i$/%	4.4	2.2	4.8
2	Experiment $\hat{f}_i$/Hz	20.5	67.2	129.2
	Calculation with considering degradation f_i/Hz	22.1	70.7	135.7
	Calculation without considering degradation $\overline{f_i}$/Hz	23.6	74.3	138.6
	Error with considering degradation $\left\|\hat{f}_i - f_i\right\| / \hat{f}_i$/%	7.8	5.2	5.0
	Error without considering degradation $\left\|\hat{f}_i - \overline{f_i}\right\| / \hat{f}_i$/%	15.1	10.6	7.3
4	Experiment $\hat{f}_i$/Hz	20.3	67.0	125.7
	Calculation with considering degradation f_i/Hz	21.3	70.6	133.5
	Calculation without considering degradation $\overline{f_i}$/Hz	23.6	74.3	138.6
	Error with considering degradation $\left\|\hat{f}_i - f_i\right\| / \hat{f}_i$/%	4.9	5.4	6.2
	Error without considering degradation $\left\|\hat{f}_i - \overline{f_i}\right\| / \hat{f}_i$/%	16.3	10.9	10.3
6	Experiment $\hat{f}_i$/Hz	19.3	66.7	121.6
	Calculation with considering degradation f_i/Hz	20.9	70.5	132.7
	Calculation without considering degradation $\overline{f_i}$/Hz	23.6	74.3	138.6
	Error with considering degradation $\left\|\hat{f}_i - f_i\right\| / \hat{f}_i$/%	8.3	5.7	9.1
	Error without considering degradation $\left\|\hat{f}_i - \overline{f_i}\right\| / \hat{f}_i$/%	22.3	11.4	14.0

was applied to the plate specimens. The theoretical resonant responses were also calculated with the same excitation amplitude used in the experiment. For the convenience of comparison, Fig. 6 presents the calculated and measured resonant responses of composite plate D at 120 °C, and Fig. 7 presents the corresponding resonant responses of composite plate E at 180 °C. Besides, the maximum calculation error in each mode of FCTP is listed in the same figures as well.

It can be seen from Figs. 6 and 7 that the calculation errors of resonant responses by considering the degradation effect at different temperatures are no more than 9.9%, which further verifies the degradation model. Besides, the amplitudes of the first three resonant responses of FCTP at different degradation time points gradually increase compared to the ones at room temperature. Meanwhile, the higher the temperature is, the more intense the resonance in each mode of FCTP. Taking the experimental results at degradation time point of 2 h as an example, the first resonant response increases from 0.0687 to 0.0797 m/s when the temperature rises from 120 to 180 °C. The reason for this intense vibration phenomenon is the stiffness softening behavior induced by thermal degradation effect, which becomes more obvious when the temperature rises.

However, the increasing trend of resonant responses of FCTP gradually becomes mild as the degradation time increases, i.e., the longer the degradation time is, the smaller influence it has on the dynamic responses. This is also reflected by the reduction of slopes in resonant response curves for different modes. The reason may be that although the softening stiffness led by degradation effect aggravating the vibration of FCTP, the structural damping still plays an important role. As the degradation time goes on, the effect of the increased damping property becomes non-negligible. Therefore, the resonant responses of FCTP show a weakened upward trend.

Journal: 11071 MS: 5232 TYPESET DISK LE CP Disp.:2019/9/6 Pages: 21 Layout: Medium

Table 8 The measured and calculated natural frequencies of composite plate E with varied degradation time at 180 °C as well as the calculation errors with and without considering degradation behavior

Time/h	Type	Mode 1	Mode 2	Mode 3
0 (Room temperature)	Experiment $\hat{f}_i$/Hz	25.3	74.0	158.3
	Calculation f_i/Hz	25.9	75.2	162.4
	Error $\left\|\hat{f}_i - f_i\right\|/\hat{f}_i/\%$	2.4	1.6	2.6
2	Experiment $\hat{f}_i$/Hz	18.2	65.3	119.3
	Calculation with considering degradation f_i/Hz	19.7	69.4	126.4
	Calculation without considering degradation $\overline{f_i}$/Hz	21.2	72.6	131.3
	Error with considering degradation $\left\|\hat{f}_i - f_i\right\|/\hat{f}_i/\%$	8.2	6.3	6.0
	Error without considering degradation $\left\|\hat{f}_i - \overline{f_i}\right\|/\hat{f}_i/\%$	16.5	11.2	10.1
4	Experiment $\hat{f}_i$/Hz	17.7	65.0	118.7
	Calculation with considering degradation f_i/Hz	19.4	68.8	123.1
	Calculation without considering degradation $\overline{f_i}$/Hz	21.2	72.6	131.3
	Error with considering degradation $\left\|\hat{f}_i - f_i\right\|/\hat{f}_i/\%$	9.6	5.8	3.7
	Error without considering degradation $\left\|\hat{f}_i - \overline{f_i}\right\|/\hat{f}_i/\%$	19.8	11.7	10.6
6	Experiment $\hat{f}_i$/Hz	17.5	65.0	117.3
	Calculation with considering degradation f_i/Hz	19.1	68.5	122.0
	Calculation without considering degradation $\overline{f_i}$/Hz	21.2	72.6	131.3
	Error with considering degradation $\left\|\hat{f}_i - f_i\right\|/\hat{f}_i/\%$	9.1	5.4	4.0
	Error without considering degradation $\left\|\hat{f}_i - \overline{f_i}\right\|/\hat{f}_i/\%$	21.1	11.7	11.9

Table 9 The measured and calculated modal shapes of the composite plate D with varied degradation time at 120 °C

Time/h	Mode 1 Experiment	Mode 1 Calculation	Mode 2 Experiment	Mode 2 Calculation	Mode 3 Experiment	Mode 3 Calculation
0	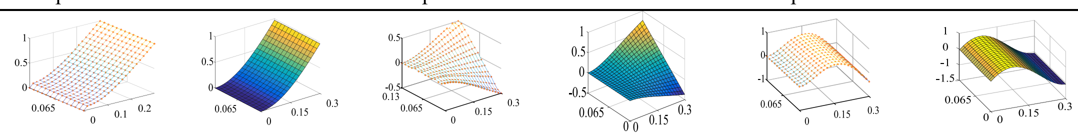					
2	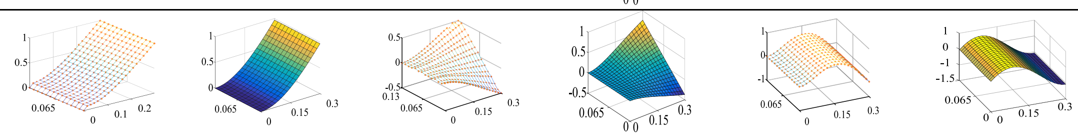					
4	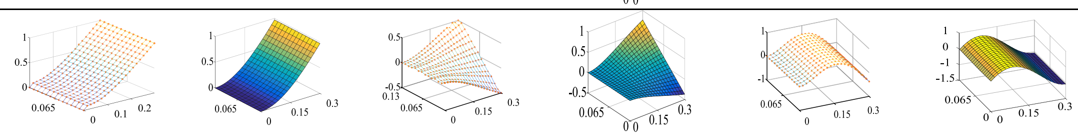					
6	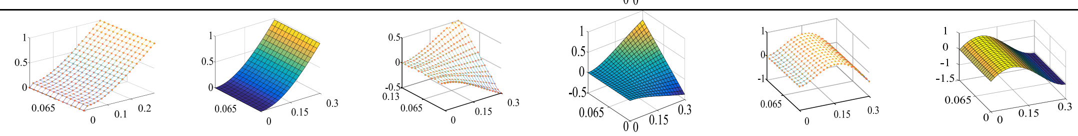					

Journal: **11071** MS: **5232** TYPESET DISK LE CP Disp.:**2019/9/6** Pages: **21** Layout: **Medium**

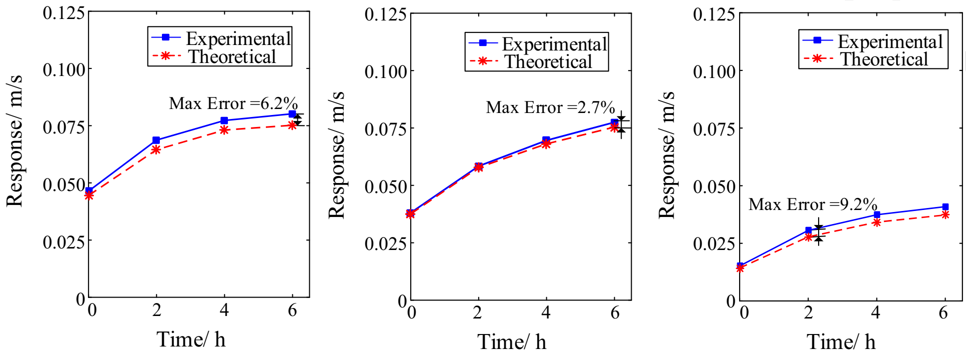

(a) Mode 1 **(b)** Mode 2 **(c)** Mode 3

Fig. 6 The first three resonant responses of composite plate *D* obtained by theoretical calculations and experimental tests with varied degradation time at 120 °C

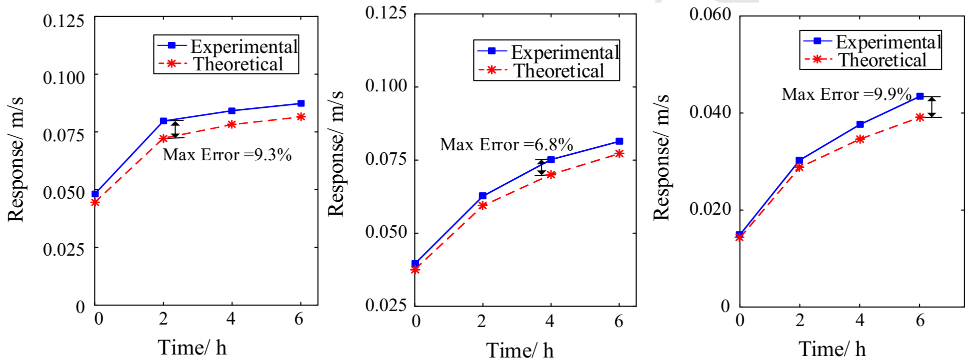

(a) Mode 1 **(b)** Mode 2 **(c)** Mode 3

Fig. 7 The first three resonant responses of composite plate *E* obtained by theoretical calculations and experimental tests with varied degradation time at 180 °C

4.5 Comparison and verification of the damping behavior

In this section, the first three modal damping ratios of composite plates *D* and *E* with varied degradation time at 120 °C and 180 °C were obtained by identifying the frequency domain data in a sine sweeping excitation test, as shown in Figs. 8a and 9a. For the convenience of comparison, the theoretical damping results of composite plates *D* and plate *E* were also obtained, as seen in Figs. 8a and 9a, where the related maximum calculation errors of the first 3 modes of FCTP are also indicated in the same figures. Besides, in order to visualize the effect of degradation time on damping property, the measured and calculated rising rates for the first three modal damping ratios of composite plate *D* and plate *E* at 120 °C and 180 °C are plotted in Figs. 8b and 9b.

It can be seen from Figs. 8a and 9a that the calculation errors of the first three modal damping ratios with considering the degradation effect at different temperatures are less than 5.0%, which further verifies the degradation model. Besides, the damping properties of FCTP at different degradation time points in thermal environment gradually increase compared to the ones at room temperature. Meanwhile, the higher the temperature is, the larger each modal damping ratio is. Taking the experimental results at degradation time point of 2 h as an example, when the temperature rises from 120 to 180 °C, the first modal damping ratio increases from 0.741 to 0.755%. The reason may be the increased energy dissipation capacity of interfacial friction in the composite plate induced by thermal degradation effect, which becomes more severe when the temperature rises.

Journal: 11071 MS: 5232 TYPESET DISK LE CP Disp.:2019/9/6 Pages: 21 Layout: Medium

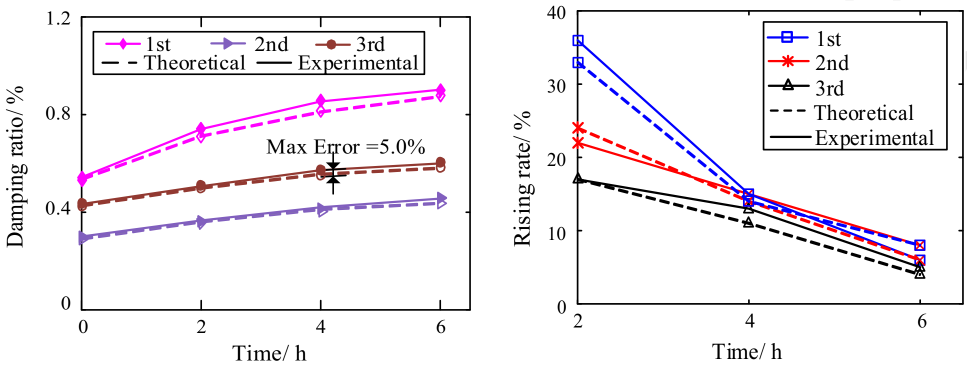

(a) The first 3 damping ratio results

(b) The rising rate of the first 3 damping ratios

Fig. 8 The first three damping ratios and the corresponding rising rate of composite plate *D* obtained by theoretical calculations and experimental tests with varied degradation time at 120 °C

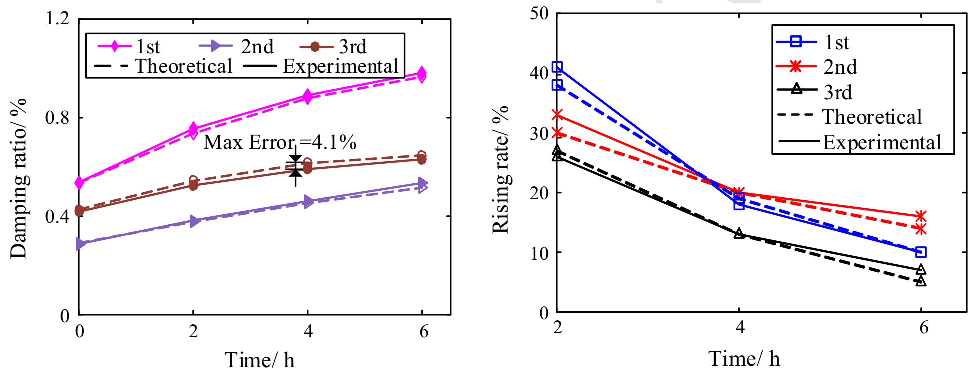

(a) The first 3 damping ratio results

(b) The rising rate of the first 3 damping ratios

Fig. 9 The first three damping ratios and the corresponding rising rate of composite plate *E* obtained by theoretical calculations and experimental tests with varied degradation time at 180 °C

However, from Figs. 8b and 9b, it can be found out that the uptrend of damping properties of FCTP declines gradually as the degradation time increases. By taking the experimental damping ratios of composite plate *D* at 120 °C as an example, when the environmental temperature is raised from room temperature to a higher temperature through the first heating process for 2 hours, the rising rates of the first three damping ratios reach to 36.2, 21.9 and 16.8%. While at the degradation time point of 4 h, those values are reduced to 15.2, 14.7 and 13.0%, and finally at the degradation time point of 6 h, are further declined to 5.6, 8.6 and 4.7%. The reason for this may be that as the degradation time continues, the energy dissipation capacity of interfacial friction in the composite plate is gradually weakened, i.e., there is less and less thermal energy being able to be converted into the friction and dissipation energy during the degradation process. In addition, from a chemical reaction point of view, it can be explained by the fact that the polymer matrix of fiber-reinforced composites is getting harder and harder due to the thermal oxidation effect [49].

5 Conclusions

In this research, a novel dynamic degradation model of FCTP subjected to thermal environment with degradation time has been established and verified. Also, the nonlinear dynamic degradation characteristics of FCTP are investigated. It can be discovered that:

Due to the stiffness softening behavior and increased energy dissipation capacity of interfacial friction of fiber-reinforced composites, the higher the temperature

Journal: 11071 MS: 5232 TYPESET DISK LE CP Disp.:2019/9/6 Pages: 21 Layout: Medium

is, the more natural frequencies of FCTP decrease, and the more on the dynamic responses and damping properties increase.

However, due to the complicated effects of thermal degradation on stiffness and material properties, as the degradation time continues, the composite thin plate structures show a slowed downward trend in changing of natural frequencies, while an upward trend in resonant responses and damping behavior becomes less and less steep.

In addition, due to that the actual thermal environment applied on FCTP is quite complicated, which not only covers the constant temperature, but also the heating and cooling stages. Therefore, the future work should consider those above factors, better to establish a more comprehensive model to describe the degradation behavior of FCTP in a quick-change thermal condition.

Acknowledgements This study was supported by the National Natural Science Foundation of China Granted Nos. 51505070, 51970530, and U1708257, the Fundamental Research Funds for the Central Universities of China Granted Nos. N160313002, N160312001, N170302001, N180302004, N180703018 and N180313006, the Scholarship Fund of China Scholarship Council (CSC) Granted No. 201806085032, and the Key Laboratory of Vibration and Control of Aero-Propulsion System Ministry of Education, Northeastern University, Granted No. VCAME201603.

Compliance with ethical standards

Conflict of interest The authors declared no potential conflicts of interest with respect to the research, authorship, and/or publication of this article.

Appendix

$$\bar{Q}_{11} = \frac{E_1^*(\Delta T,t)}{1-\mu_{12}\mu_{21}}\cos^4\theta_k + 2\frac{\mu_{12}E_1^*(\Delta T,t)}{1-\mu_{12}\mu_{21}}\sin^2\theta_k\cos^2\theta_k$$

$$+4G_{12}^*(\Delta T,t)\sin^2\theta_k\cos^2\theta_k + \frac{E_2^*(\Delta T,t)}{1-\mu_{12}\mu_{21}}\sin^4\theta_k$$

$$\bar{Q}_{12} = \left(\frac{E_1^*(\Delta T,t)+E_2^*(\Delta T,t)}{1-\mu_{12}\mu_{21}} - 4G_{12}^*(\Delta T,t)\right)\sin^2\theta_k\cos^2\theta_k$$

$$+\frac{\mu_{12}E_1^*(\Delta T,t)}{1-\mu_{12}\mu_{21}}\left(\sin^4\theta_k+\cos^4\theta_k\right)$$

$$\bar{Q}_{22} = \frac{E_1^*(\Delta T,t)}{1-\mu_{12}\mu_{21}}\sin^4\theta_k + 2\frac{\mu_{12}E_1^*(\Delta T,t)}{1-\mu_{12}\mu_{21}}\sin^2\theta_k\cos^2\theta_k$$

$$+4G_{12}^*(\Delta T,t)\sin^2\theta_k\cos^2\theta_k + \frac{E_2^*(\Delta T,t)}{1-\mu_{12}\mu_{21}}\cos^4\theta_k$$

$$\bar{Q}_{16} = \left(\frac{(1-\mu_{12})E_1^*(\Delta T,t)}{1-\mu_{12}\mu_{21}} - 2G_{12}^*(\Delta T,t)\right)\sin\theta_k\cos^3\theta_k$$

$$+\frac{\mu_{12}E_1^*(\Delta T,t)-E_2^*(\Delta T,t)}{1-\mu_{12}\mu_{21}}\sin^3\theta_k\cos\theta_k$$

$$+2G_{12}^*(\Delta T,t)\sin^3\theta_k\cos\theta_k$$

$$\bar{Q}_{26} = \left(\frac{(1-\mu_{12})E_1^*(\Delta T,t)}{1-\mu_{12}\mu_{21}} - 2G_{12}^*(\Delta T,t)\right)\sin^3\theta_k\cos\theta_k$$

$$+\frac{\mu_{12}E_1^*(\Delta T,t)-E_2^*(\Delta T,t)}{1-\mu_{12}\mu_{21}}\sin\theta_k\cos^3\theta_k$$

$$+2G_{12}^*(\Delta T,t)\sin\theta_k\cos^3\theta_k$$

$$\bar{Q}_{66} = \frac{(1-2\mu_{12})E_1^*(\Delta T,t)+E_2^*(\Delta T,t)}{1-\mu_{12}\mu_{21}}\sin^2\theta_k\cos^2\theta_k$$

$$-2G_{12}^*(\Delta T,t)\sin^2\theta_k\cos^2\theta_k$$

$$+G_{12}^*(\Delta T,t)\left(\sin^4\theta_k+\cos^4\theta_k\right)$$

References

1. Jones, R.M.: Mechanics of composite materials. Scripta Book Company, Washington (1975)
2. Vinson, J.R., Sierakowski, R.L.: The Behavior of Structures Composed of Composite Materials. Springer, Heidelberg (2006)
3. Leyens, C., Kocian, F., Hausmann, J., et al.: Materials and design concepts for high performance compressor components. Aerosp. Sci. Technol. **7**(3), 201–210 (2003)
4. Russellstevens, M., Todd, R., Papakyriacou, M.: The effect of thermal cycling on the properties of a carbon fibre reinforced magnesium composite. Mater. Sci. Eng. A **397**(1), 249–256 (2005)
5. Ray, B.C.: Temperature effect during humid ageing on interfaces of glass and carbon fibers reinforced epoxy composites. J. Colloid Interface Sci. **298**(1), 111–117 (2006)
6. Jun, L., Yuchen, B., Peng, H.: A dynamic stiffness method for analysis of thermal effect on vibration and buckling of a laminated composite beam. Arch. Appl. Mech. **87**(8), 1–21 (2017)
7. Chung, K., Seferis, J.C., Nam, J.D.: Investigation of thermal degradation behavior of polymeric composites: prediction of thermal cycling effect from isothermal data. Compos. Part A **31**(9), 945–957 (2000)
8. Jeyaraj, P., Ganesan, N., Padmanabhan, C.: Vibration and acoustic response of a composite plate with inherent material damping in a thermal environment. J. Sound Vib. **320**(1), 322–338 (2009)
9. Geng, Q., Li, H., Li, Y.: Dynamic and acoustic response of a clamped rectangular plate in thermal environments: experiment and numerical simulation. J. Acoust. Soc. Am. **135**(5), 2674–2682 (2014)
10. Thwe, M., Liao, K.: Effects of environmental aging on the mechanical properties of bamboo-glass fiber reinforced polymer matrix hybrid composites. Compos. Part A Appl. Sci. Manuf. **33**(1), 43–52 (2002)
11. Wolfrum, J., Eibl, S., Lietch, L.: Rapid evaluation of long-term thermal degradation of carbon fibre epoxy composites. Compos. Sci. Technol. **69**(3–4), 523–530 (2009)
12. Rezaei, F., Yunus, R., Ibrahim, N.A.: Effect of fiber length on thermomechanical properties of short carbon fiber reinforced polypropylene composites. Mater. Des. **30**(2), 260–263 (2009)

13. Kahirdeh, A., Khonsari, M.: Criticality of degradation in composite materials subjected to cyclic loading. Compos. Part B Eng. **61**(5), 375–382 (2014)
14. Horn, W.J., Soeganto, A., Shaikh, F.M.: Degradation of mechanical properties of advanced composites exposed to aircraft environment. AIAA J. **27**(10), 1399–1405 (2015)
15. McManus, H.: Stress and damage in polymer matrix composite materials due to material degradation at high temperatures. In: 35th Structures, Structural Dynamics, and Materials Conference, pp. 1395–1402 (1996)
16. Chung, K., Seferis, J.C., Nam, J.D.: Investigation of thermal degradation behavior of polymeric composites: prediction of thermal cycling effect from isothermal data. Compos. Part A Appl. Sci. Manuf. **31**(9), 945–957 (2000)
17. Zinchenko, V.I., Nesmelov, V., Gol'din, V.D.: Prediction of thermal degradation of thermoprotective materials on the basis of their composition and properties of components. Combust. Explos. Shock Waves **41**(1), 57–63 (2005)
18. Wang, Y.C., Wong, P.M.H., Kodur, V.: An experimental study of the mechanical properties of fibre reinforced polymer (FRP) and steel reinforcing bars at elevated temperatures. Compos. Struct. **80**(1), 131–140 (2007)
19. Dawood, M., Rizkalla, S.: Environmental durability of a CFRP system for strengthening steel structures. Constr. Build. Mater. **24**(9), 1682–1689 (2010)
20. Lafarie-Frenot, M.C., Grandidier, J.C., Gigliotti, M., et al.: Thermo-oxidation behaviour of composite materials at high temperatures: a review of research activities carried out within the COMEDI program. Polym. Degrad. Stab. **95**(6), 965–974 (2010)
21. Upadhyaya, P., Singh, S., Roy, S.: A mechanism-based multi-scale model for predicting thermo-oxidative degradation in high temperature polymer matrix composites. Compos. Sci. Technol. **71**(10), 1309–1315 (2011)
22. Bojja, R., Chandra, A., Jagannathan, N., et al.: Micromechanics modeling and prediction of stiffness degradation behavior of a fiber reinforced polymer nanocomposite under block amplitude fatigue loads. Trans. Indian Inst. Met. **69**(2), 1–5 (2016)
23. Khalili, S.M.R., Najafi, M., Eslami-Farsani, R.: Effect of thermal cycling on the tensile behavior of polymer composites reinforced by basalt and carbon fibers. Mech. Compos. Mater. **52**(6), 807–816 (2017)
24. Ndiaye, E.B., Duflo, H., Maréchal, P., et al.: Thermal aging characterization of composite plates and honeycomb sandwiches by electromechanical measurement. J. Acoust. Soc. Am. **142**(6), 3691–3702 (2017)
25. Guo, J., Wang, M., Li, L., et al.: Effects of thermal-oxidative aging on the flammability, thermal degradation kinetics and mechanical properties of DBDPE flame retardant long glass fiber reinforced polypropylene composites. Polym. Compos. **39**(S3), E1733–E1741 (2018)
26. Huang, X.L., Shen, H.S.: Nonlinear vibration and dynamic response of functionally graded plates in thermal environments. Int. J. Solids Struct. **41**(9–10), 2403–2427 (2004)
27. Melo, J.D., Radford, D.W.: Time and temperature dependence of the viscoelastic properties of CFRP by dynamic mechanical analysis. Compos. Struct. **70**(2), 240–253 (2005)
28. Duc, N.D., Cong, P.H., Quang, V.D.: Nonlinear dynamic and vibration analysis of piezoelectric eccentrically stiffened FGM plates in thermal environment. Int. J. Mech. Sci. **115**, 711–722 (2016)
29. Wu, D., Wang, Y., Shang, L., et al.: Experimental and computational investigations of thermal modal parameters for a plate-structure under 1200 °C high temperature environment. Measurement **94**, 80–91 (2016)
30. Jakkamputi, L.P., Rajamohan, V.: Dynamic characterization of CNT-reinforced hybrid polymer composite beam under elevated temperature-an experimental study. Polym. Compos. **40**(2), 464–470 (2017)
31. Liu, Z., Guan, Z., Liu, F., et al.: Time-temperature dependent mechanical properties of cured epoxy resin and unidirectional CFRP. In: 2017 8th International Conference on Mechanical and Aerospace Engineering (ICMAE). IEEE, pp. 113–117 (2017)
32. Bai, Y., Yu, K., Zhao, J., et al.: Experimental and simulation investigation of temperature effects on modal characteristics of composite honeycomb structure. Compos. Struct. **201**, 816–827 (2018)
33. Tsotsis, T.K., Keller, S., Lee, K., et al.: Aging of polymeric composite specimens for 5000 hours at elevated pressure and temperature. Compos. Sci. Technol. **61**(1), 75–86 (2001)
34. Guo, Z.S., Feng, J., Wang, H., et al.: A new temperature-dependent moduli model of glass/epoxy composite at elevated temperatures. J. Compos. Mater. **47**(26), 3303–3310 (2013)
35. Montalvão, D., Cláudio, R., Ribeiro, A.M.R., et al.: Experimental measurement of the complex Young's modulus on a CFRP laminate considering the constant hysteretic damping model. Compos. Struct. **97**, 91–98 (2013)
36. Li, H., Niu, Y., Mu, C., et al.: Identification of loss factor of fiber-reinforced composite based on complex modulus method. Shock Vib. **2017**, (2017) 4
37. Hyer, M.W.: Stress Analysis of Fiber-Reinforced Composite Materials. DEStech Publications Inc, Lancaster (2009)
38. Mallick, P.K.: Fiber-Reinforced Composites: Materials, Manufacturing, and Design. CRC Press, Boca Raton (2007)
39. Sun, W., Liu, Y., Li, H., et al.: Determination of the response distributions of cantilever beam under sinusoidal base excitation. J. Phys. Conf. Ser. **448**(1), 1–11 (2013)
40. Grover, N., Maiti, D.K., Singh, B.N.: A new inverse hyperbolic shear deformation theory for static and buckling analysis of laminated composite and sandwich plates. Compos. Struct. **95**, 667–675 (2013)
41. Thai, H.T., Choi, D.H.: A simple first-order shear deformation theory for laminated composite plates. Compos. Struct. **106**, 754–763 (2013)
42. Poli, R.: Particle swarm optimization—an overview. Swarm Intell. **1**(1), 33–57 (2007)
43. Cui, Q., Li, Q., Li, G., et al.: Globally-optimal prediction-based adaptive mutation particle swarm optimization. Inf. Sci. **418–419**, 186–217 (2017)
44. Martinez, W.L., Martinez, A.R., Solka, J.: Exploratory Data Analysis with MATLAB. Chapman and Hall, Boca Raton (2017)
45. Li, H., Chang, Y., Xu, Z., et al.: Modal shape measurement of fiber-reinforced composite plate with high efficiency and precision based on laser linear scanning method. Meas. Control **51**(9–10), 470–487 (2018)

46. Li, H., Zhu, M., Xu, Z., et al.: The influence on modal parameters of thin cylindrical shell under bolt looseness boundary. Shock Vib. **2016**, 1–15 (2016)
47. Dogan, A., Atas, C.: Variation of the mechanical properties of E-glass/epoxy composites subjected to hygrothermal aging. J. Compos. Mater. **50**(5), 637–646 (2016)
48. Li, H., Wu, H., Zhang, T., et al.: Analysis and verification of vibration response of fiber-reinforced cantilever composite thin plate in thermal vibration environment. Acta Armamentarii **39**, 373–382 (2018)
49. Leveque, D., Schieffer, A., Mavel, A., et al.: Analysis of how thermal aging affects the long-term mechanical behavior and strength of polymer–matrix composites. Composi. Sci. Technol. **65**(3–4), 395–401 (2005)

Journal: 11071
Article: 5232

Author Query Form

Please ensure you fill out your response to the queries raised below and return this form along with your corrections

Dear Author

During the process of typesetting your article, the following queries have arisen. Please check your typeset proof carefully against the queries listed below and mark the necessary changes either directly on the proof/online grid or in the 'Author's response' area provided below

Query	Details required	Author's response
1.	Kindly check and confirm whether the corresponding author and affiliation is correctly identified.	
2.	Please check and confirm that the authors and their respective affiliations have been correctly identified and amend if necessary.	
3.	As Refs [11] and [19] are same, we have deleted the duplicate reference and renumbered accordingly. Please check and confirm.	
4.	Please provide complete details for the Ref. [36].	